

PAPER • OPEN ACCESS

Potential of Mini Gurney Flaps as a Retrofit to Mitigate the Performance Degradation of Wind Turbine Blades Induced by Erosion

To cite this article: Francesco Papi *et al* 2022 *J. Phys.: Conf. Ser.* **2265** 032046

View the [article online](#) for updates and enhancements.

You may also like

- [Rate-programming of nano-particulate delivery systems for smart bioactive scaffolds in tissue engineering](#)
Mohammad Izadifar, Azita Haddadi, Xiongbiao Chen *et al.*
- [Stress-induced elastic modulus evolution in metallic glasses](#)
Wei-Bing Liao, Zhi-Yuan Liu, Chun-Yan Yu *et al.*
- [Towards closed strings as single-valued open strings at genus one](#)
Jan E Gerken, Axel Kleinschmidt, Carlos R Mafra *et al.*



The Electrochemical Society
Advancing solid state & electrochemical science & technology

243rd ECS Meeting with SOFC-XVIII

More than 50 symposia are available!

Present your research and accelerate science

Boston, MA • May 28 – June 2, 2023

[Learn more and submit!](#)

Potential of Mini Gurney Flaps as a Retrofit to Mitigate the Performance Degradation of Wind Turbine Blades Induced by Erosion

Francesco Papi¹, Pier Francesco Melani¹, Jörg Alber², Francesco Balduzzi¹, Giovanni Ferrara¹, Christian Navid Nayeri², Alessandro Bianchini^{1,*}

¹ Department of Industrial Engineering, Università degli Studi di Firenze, Via di Santa Marta 3, 50139, Firenze, Italy.

² Technische Universität Berlin, Hermann-Föttinger-Institut (HFI), Müller-Breslau Str. 8, 10623, Berlin, Germany.

* Corresponding author: alessandro.bianchini@unifi.it

Abstract. Leading edge erosion of wind turbine blades is still an important challenge for wind energy professionals, both at research and industrial level. While the efficiency and durability of materials and coatings are improving rapidly, it is important to explore innovative solutions at the aerodynamic design level to mitigate the adverse effects of surface erosion. For that, a preliminary analysis on the use of Mini Gurney Flaps (MGFs) is presented in the study. High-fidelity Computational Fluid Dynamic (CFD) simulations are used to evaluate the impact of severe leading edge (LE) erosion on the performance of the FFAW3-241 airfoil on the rotor blade of the DTU 10-MW Reference Wind Turbine, which is used as test case. CFD lift and drag polars of the eroded airfoil show that MGFs are able to partially recover aerodynamic efficiency caused by erosion; this suggested evaluating their use as a retrofit solution for blades that already experienced leading edge erosion damage. When tested on the DTU 10MW RWT blade, results show how, if sized correctly, MGFs perform as predicted: the lift curve is shifted back to its design value and performance is improved with respect to the eroded blade. Moreover, as one would expect, higher than optimal MGFs resulted in excessive lift increases and thus decreased performance, even in the case of LE-erosion. Although these devices behave as intended however, based on the results of this paper, performance decreases are noted at high tip-speed-ratios (TSR), due to the blade operating in off-design conditions.

Keywords: LE erosion, HAWT, Mini Gurney Flap

1. Introduction and objectives of the study

Leading edge erosion of wind turbine blades is still one of the most challenging issue for wind turbine professionals [1]. The deterioration of blade surface has an adverse impact on performance and structural integrity of turbines [2]. Moreover, recent studies have shown that erosion levels are often higher and taking place earlier than expected [3].



Erosion usually starts with the formation of small pits on the leading-edge. These defects then progressively expand, until they merge into wider and deeper gauges. As the surface continues to be repeatedly impacted, the protective external layers of the blade start to crack and chip [2]. This phenomenon is referred to as “delamination” [4]. Erosion is typically observed in the outer parts of the rotor, in virtue of the higher relative speed [5]. In terms of impact on blade section aerodynamics, experiments and simulations show that erosion leads to a decrease of the lift coefficient (C_L) and a corresponding increase of the drag coefficient (C_D) [6], i.e., to a detriment of the glide ratio of a given airfoil. Erosion also typically causes anticipated static stall angles. While the efficiency and durability of materials and coatings are improved constantly [7], novel solutions at design level can be explored to mitigate the aerodynamic impact of erosion.

Within this context, this study presents a preliminary analysis on the potential use of Mini Gurney Flaps (MGFs) to this scope. Gurney Flaps (GFs) are thin tabs that are attached at the trailing edge of an airfoil in order to increase lift in pre-stall operation, while accepting small drag penalties. The concept of Gurney Flaps is well studied. An important example of a GF proposal in large horizontal axis turbines is the blade design of the DTU 10MW Reference Wind Turbine (RWT) by the Danish Technical University (DTU) [8]. The inner blade part alongside the local rotor radius of $5\%R < r < 40\%R$ was there equipped with wedge-shaped GFs including heights of $3.5\%c$, $2.5\%c$ and $1.3\%c$, respectively. Bak et al. claim significant aerodynamic performance improvements, especially on relatively thick airfoils. More recently, Alber et al. [9] presented a study on the impact of the so-called Mini Gurney Flaps for use on HAWTs, i.e. GF with heights that are significantly smaller than the airfoil boundary layer. In this way, the lift increase is more pronounced in relation to the drag penalty.

To evaluate the potential of MGFs in mitigating the loss in airfoil performance due to leading edge erosion, high-fidelity Computational Fluid Dynamic (CFD) simulations are first used in the study to evaluate the impact of a severe erosion on the performance of the FFAW3-241 airfoil. The CFD model is calibrated using experimental tests of the DU97W-300 airfoil with and without the presence of a MGF [9], as explained in detail in section 2.3. The calculated lift and drag polars are then applied to the DTU 10-MW RWT, which is used as rotor test case. Airfoil polars calculated with CFD are eventually analyzed to evaluate the potential of MGFs as a retrofit for eroded blades in the field. This is done using the full aero-servo-elastic OpenFAST [9] model of the DTU 10-MW RWT. Because MGFs are used as a retrofit device in the current work, their potential impact on the erosion process at the leading edge is neglected. Further investigation on the interactions of the flow-field changes induced by MGFs and the leading edge erosion process are left as future developments.

2. Methods

2.1. Erosion Modelling

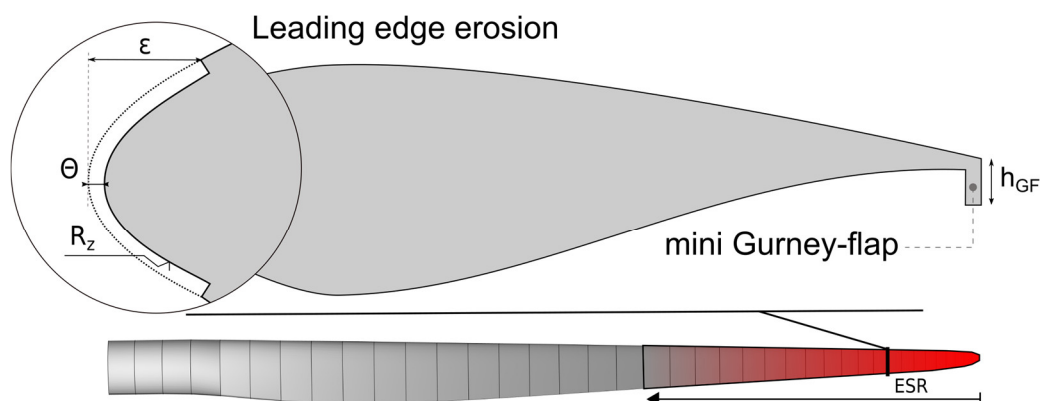


Figure 1. Erosion modelling parameters. Example of resulting intensity of erosion-related performance decrease along the blade in red.

In the study, erosion is modelled by means of four independent parameters: erosion depth θ , extension in percentage of the blade chord ε , total roughness of the airfoil nose R_z and extension along the blade span ESR. θ and R_z are expressed in millimeters. A schematic representation of these parameters is shown in Figure 1. It must be noted that in the blades affected by erosion damage, the parameters θ , ε and R_z are not related to the dimensions of the local airfoil section, but imposed as constant values along the blade span. Therefore, as the blade chord decreases going towards the rotor tip, the influence of these parameters becomes more relevant. As erosion damage is related to the relative velocity of each blade section in operation, this approach allows to model the increase of the damage towards blade tip, as shown in Figure 1. The effectiveness of such modelling strategy was validated in a previous work by some of the authors [2].

Table 1. Erosion parameters selected for the analysis (severe erosion).

Parameter	ε [-]	θ [mm]	R_z [mm]	ESR
Value	6.69	1.8817	0.3222	0.302

In the present study, a *severe* level of damage was selected from the data points that were simulated in [2]. The corresponding four erosion parameters are reported in Table 1. In order to effectively account for the variations in the chord length and thus the Reynolds number along the blade, lift and drag coefficients were calculated for three blade sections located at different span locations, adjusting the inflow velocity accordingly (see Table 2). To the purpose, a dedicated blade-resolved CFD model was employed, as detailed in Section 2.2.

For each blade section three GF heights are tested: 0.25%, 0.5% and 1% of blade chord. These values were selected based on previous research [9], which indicates that to be effective, MGFs need to be immersed deeply into the blade boundary layer at the trailing edge. If this condition is not met, the increases in C_D typically outweigh the increases in C_L , leading to sub-optimal performance. Determining the height of the blade's boundary layer nonetheless is not straightforward, due to the complex flow patterns that are created by the presence of the airfoil itself. In this work, the procedure highlighted in [9] was adopted, quickly estimating the boundary layer height as:

$$\delta = \theta \left(3.15 + \frac{1.72}{\left(\frac{\delta^*}{\theta}\right)^{-1}} \right) + \delta^* \quad (1)$$

where δ^* is the boundary layer displacement thickness and θ is the momentum thickness. These two quantities were estimated with XFOIL [10], obtaining for instance a boundary layer thickness of approximately 0.97% chord at the design AoA of 8° for section #2 (Table 2). Given an appropriate boundary layer height in the order of one quarter of the turbulent boundary layer thickness at trailing edge [9], this corresponds to a MGF height of 0.25%*c*, which is the smallest size chosen for this analysis. Two additional MGF heights, which still result in the MGF being enclosed in the turbulent boundary layer but are higher than the suggested optimum are also tested. This is due to the fact that in the presence of erosion, the boundary layer thickness is expected to increase.

Table 2. Simulated blade sections

Section	#1	#2	#3
Blade span [%]	70.1	94	100
<i>c</i> [m]	3.62	2.02	0.60
<i>u</i> [m/s]	63.38	84.30	89.64
Reynolds	14×10^6	11×10^6	3.5×10^6
MGF height	0.25-1% <i>c</i>	0.25-1% <i>c</i>	0.25-1% <i>c</i>

2.2. CFD airfoil simulations

Due to the complexity of eroded geometries, especially if including MGFs, panel methods traditionally used for airfoil polar generation are not adequate. To overcome this, Computational Fluid Dynamics (CFD) is used. In particular, a two-dimensional unsteady Reynolds-Averaged Navier-Stokes (URANS) approach has been used. The polar data for the eroded airfoils equipped with mini-GF was achieved with a dedicated two-dimensional unsteady CFD model, by applying a *ramp-up* motion to the airfoil in the desired AoA range [11]. Ramp-up speed Ω was selected in such a way that the airfoil reduced frequency $k=\Omega c/(2u) \leq 0.001$, to avoid dynamic effects. Although computationally more expensive, the unsteady formulation was in fact required by the MGF, which - especially at the lower AoA - is characterized by a high-frequency vortex shedding [11]. The ANSYS® FLUENT® (v. 20.2) solver, based on a combination of the consolidated numerical approaches developed for GF [11] and LE erosion [2] simulations is used. The *coupled* algorithm for pressure-velocity coupling, the 2nd order upwind scheme for both RANS and turbulence equations and the second order bounded scheme for time marching were used. For turbulence closure, a dedicated sensitivity analysis, not reported here for brevity, was carried out, resulting in the selection of the *4 Eqs. transition γ - Re_θ model* [12] with the original settings of the solver. This choice was supported by the previous experience of some of the authors on LE erosion [2]. This choice was crucial to achieving good results when validating the CFD approach. In fact, especially for thick airfoils such as the DU-97-W-300, the presence of a laminar boundary layer at the leading-edge of the blade on airfoil performance is still persistent in such flow conditions [13].

The computational domain has an *open field* configuration, with an overall extent of $L=60c$ and a width of $W=40c$ to avoid blockage effects. As shown in Figure 2a, the latter is separated into two parts: an external bullet-shaped region and an internal circular one, containing the airfoil. The adoption of a *sliding interface* allows the rotation of the inner domain, in order to vary the angular position during the simulation according to a specific user-defined profile. At its boundaries, the standard *far field* boundary conditions for external flows are applied, i.e.: uniform velocity, turbulence intensity and length scale at the inlet, ambient pressure at the outlet. The non-eroded portion of the blade surface is modeled instead as smooth *no slip* wall.

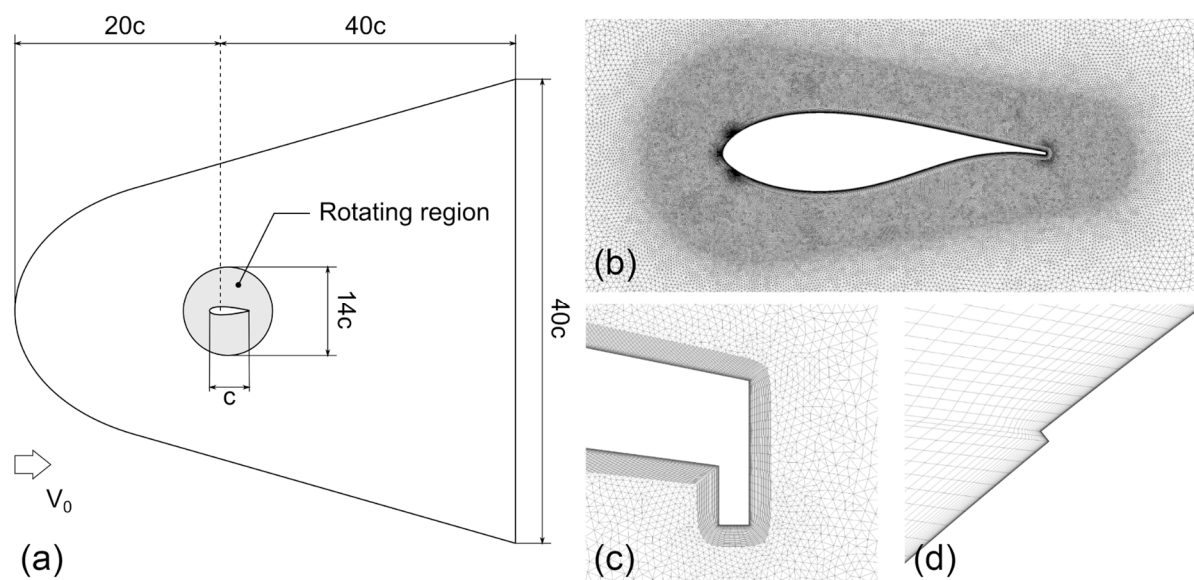


Figure 2. Details of the mesh for airfoil simulations: a) computational domain b) airfoil c) MGF d) end of the LE erosion zone.

An unstructured hybrid mesh was employed. In order to optimize the overall number of mesh elements and their distribution, local refinements were applied in proximity of the airfoil and its wake (see Figure 2b). As shown in Figure 2d, an O-grid of quadrilateral elements was used around the blade boundary layer: the height of the wall-adjacent cell is able to guarantee a value of the dimensionless wall distance (y^+) lower than 1, while the total number of layers is 40. At the blade trailing edge, a higher mesh resolution was necessary due to the aforementioned high-frequency vortex shedding phenomenon occurring at the lower AoAs, as shown in Figure 2c. It must be noted how this feature also limited the simulation timestep, which was selected to comply with both the GF shedding frequency and the airfoil ramp-up one. The overall mesh sizing is determined based on previous studies by the authors where CFD simulations of airfoils with GFs and leading-edge erosion were performed [2,11,14], however the number of elements along the blade surface was conservatively increased to 1000 in order to have sufficient resolution at both leading and trailing edge.

2.3. Validation

The proposed approach was also validated against experimental data provided by Alber et al. [9]. The wind tunnel experiments were conducted in the closed-loop wind tunnel of the HFI at the TU Berlin. The tested wing has a chord of 0.6 meters and a span on 1.54m. Two smooth end plates are mounted on each side of the wing in order to minimize the effects of the wind tunnel boundary layer. Lift forces were determined by means of a six-component force balance and drag forces using a wake-rake. At stall, however, measurements are not reliable since the wind tunnel blockage effects become dominant. Therefore drag readings beyond the stall point are shown in small symbols in Figure 3.

Figure 3 shows the results of the calibrated CFD model with respect to experimental data in terms of lift, drag and aerodynamic efficiency. Good agreement regarding the pre-stall lift coefficients up to about 13° , which is approximately the stall point in the wind tunnel data. In this region, a slight underestimation of drag is also noted, which leads to a slight overestimation of the lift-to-drag ratio. Furthermore, it is apparent that the simulations correctly model the shift of the curve due to the presence of the MGF. The numerical model tends, however, to delay the airfoil stall point with respect to the measurements. This value is notoriously difficult to predict accurately with CFD simulations, especially when simulating a thick airfoil such as the DU97W-300. In fact, the stall angle often depends on case-specific parameters that are difficult to control such as, for instance, the tested sections roughness, interaction with wind tunnel walls, or turbulence intensity. At the same time, this issue only marginally impacts the results of present study, which is basically comparative and was made on a pitch-regulated blade, which is designed to operate in the linear region, where excellent agreement was achieved.

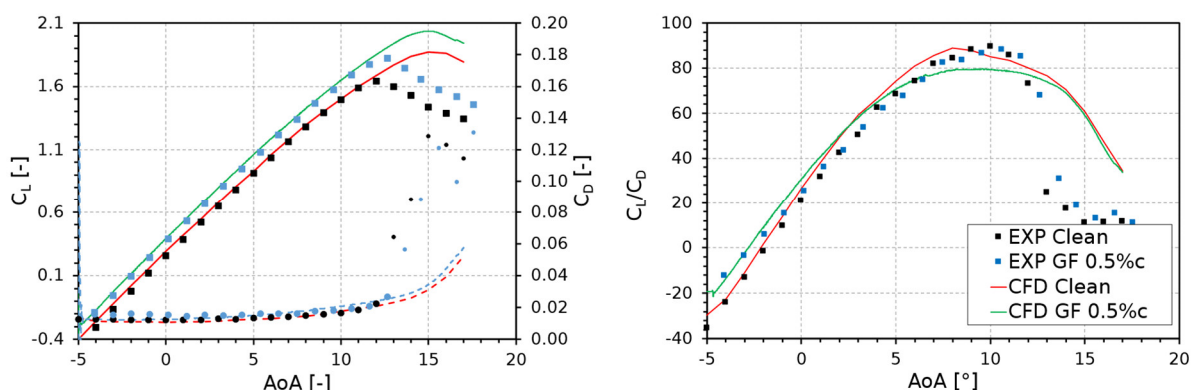


Figure 3. Lift, drag and lift-to-drag ratio of CFD airfoil model of DU97-W-300 compared to experimental data from [9] at Reynolds = $1.5 \cdot 10^6$.

2.4. Turbine model in OpenFAST

The DTU 10MW RWT turbine is modelled using OpenFAST [15]. The used model is the same as the one used by the authors in [2], where it is explained in detail and the modelling approach is validated against other literature numerical data.

Aerodynamics are solved using the Blade Element Momentum (BEM) method in the *Aerodyn* [16] module. Correction for high-induction, tip and root losses, and skewed inflow are included. Structural dynamics are handled by the *Elastodyn* module. The blades and the tower are modelled using a modal approach, where the deflections of the components are computed through linear superposition of pre-determined mode shapes. The structural properties of the eroded blades are left unchanged as erosion damage mainly affects the blade leading-edge, which is generally regarded as a non-critical part of the blade structure, since its stiffness is mainly provided by spar caps and shear webs inside the blades. Moreover, erosion damage mainly affects the outer layer of the blade shell (Gelcoat and epoxy) which are not structurally stressed components of the layout.

For the present study the turbine is simulated assuming ideal conditions. No turbulence or skewed inflow is considered, only wind shear effects are modelled using the power-law with an exponent of 0.2. Aerodynamic properties of each section are calculated based on the simulated lift and drag coefficients, linearly interpolating the input data to section different than the ones defined in Table 2.

3. Results

In Section 3.1 the lift and drag coefficients of the eroded airfoil are determined. Next, the effect of retrofit MGFs is discussed with respect to the undamaged airfoil performance. In Section 3.2 the polar coefficients are used for the simulation of the DTU 10MW blade.

3.1. Airfoil aerodynamics

The Lift and Drag coefficients are computed for three blade sections, see Table 2. In all cases, LE erosion causes a significant decrease in lift, and an even more significant increase in drag. Consequently, the lift-to-drag ratio of the eroded blade is decreased to approximately 2/3 of its original value at blade tip. In all three cases, the application of a MGF leads to the same effects: C_L in the pre-stall region increases significantly. However, due to the drag coefficients, the lift to drag ratio is only slightly improved, as shown in Figure 4 and Table 3. The maximum C_L/C_D for the three blade sections and GF heights as well as the relative variation with respect to the eroded section with no MGF and the angle of attack where maximum C_L/C_D is recorded is shown in Table 3. Maximum L/D is predicted between 5.5° and 9° AoA, very close to the operating AoA at these outer blade sections where it is important, from an aerodynamic design standpoint, to maximize this parameter.

As reported in Table 3, in blade sections #1 and #2 the most advantageous MGF in terms of maximum C_L/C_D is the 0.5c configuration, which allows for an increase in the aerodynamic efficiency of approximately 3.7% and 5.4% respectively. For the tip section (#3) the MGF with 1%c height allows for the greatest improvement in aerodynamic efficiency with a nearly 10% increase with respect to the value for the damaged airfoil. For sections #1 and #2 however, the most improvements in airfoil efficiency are noted for the MGF with 0.5% c height.

It is worth specifying that for all three blade sections, MGF with 0.25%c height increases lift coefficient of the damaged airfoils to be very close to that of the clean airfoil in the linear region. This is the desired effect for these devices when they are used as retrofit as will be explained in the following section. On the other hand, MGFs of 0.5% and 1% c in height increase C_L beyond the values of the clean blade.

In conclusion, from an aerodynamic standpoint, the application of a MGF to an eroded blade section is beneficial as all three simulated heights for all three blade sections produce an increase in sectional lift-to-drag ratio together with a significant increase in lift coefficient.

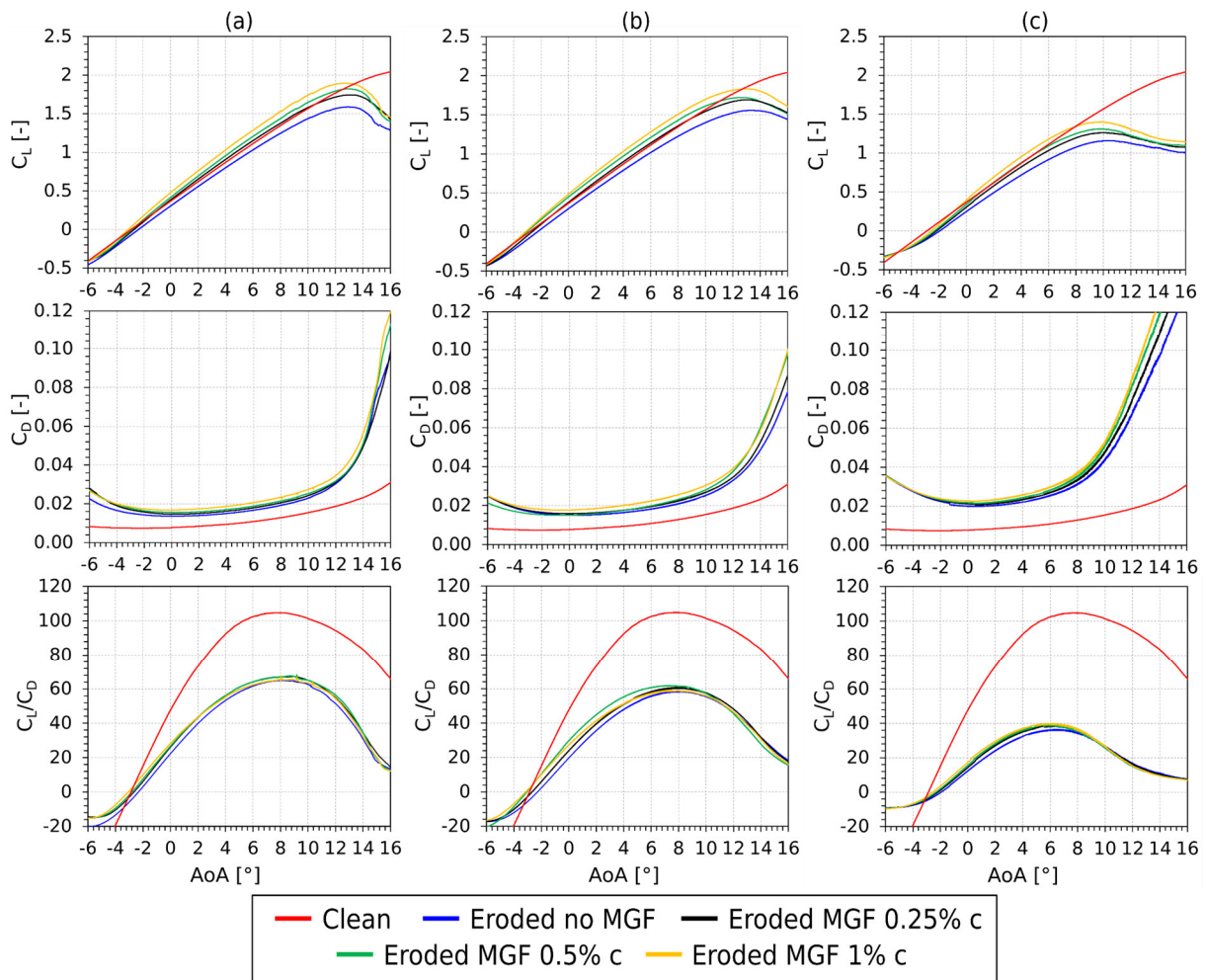


Figure 4. Lift, Drag and Lift to Drag ratio characteristics for the three simulated blade sections (FFAW3-241 airfoil at Re number ranging from $3.5 \cdot 10^6$ to $14 \cdot 10^6$) Column (a): most inner section (section 1). Column (b): intermediate section (section 2). Column (c): most tip section (section 3). Reference undamaged curve is calculated with the same inflow conditions as Section 2.

Table 3. Simulated blade sections

	GF height	NO GF	0.25% c	0.5% c	1% c
sec. 1	max Cl/Cd	65.68	67.32	68.12	67.60
	$\Delta Cl/Cd$	-	2.51%	3.72%	2.93%
	AoA max Cl/Cd	8.42	8.76	9.18	8.04
sec. 2	max Cl/Cd	58.67	60.75	61.83	59.11
	$\Delta Cl/Cd$	-	3.56%	5.39%	0.76%
	AoA max Cl/Cd	8.03	7.98	7.78	7.51
sec. 3	max Cl/Cd	36.48	38.57	38.95	39.95
	$\Delta Cl/Cd$	-	5.75%	6.78%	9.53%
	AoA max Cl/Cd	6.60	5.95	5.67	5.72

3.2. Turbine Performance

If the aerodynamic coefficients calculated applying a retrofit MGF to the damaged blade sections are applied to the DTU 10MW RWT blade as described in section 2.4. The produced power output of the turbine decreases with respect to the eroded blade for most wind speeds. This is shown clearly in Figure 5a, where the relative power variation with respect to the undamaged configuration is shown for the damaged blade and the damaged blade with the various MGF heights. With the exception of 8, 9 and 10m/s wind speeds, where an ever so slight increase in performance respect to the eroded configuration can be noted for the blade with a 0.25%*c* MGF height, all MGF heights produce larger decreases in power than the eroded configuration and are not able to partially compensate erosion damage. This is apparently in contrast to the results discussed in Section 3.1, where a recovery in airfoil glide ratio was noted. Analyzing figure 5b, peak C_p at $TSR=7$ increases from 0.448 of the eroded configurations to 0.450 when applying the 0.25%*c* MGF and 0.4497 for the 0.5% *c* MGF. For the 1%*c* MGF a reduction in peak C_p to 0.445 is predicted. All these values are well below the power coefficient of the undamaged turbine, predicted to be 0.469. This explains the slight increases in power production for the 0.25% MGF between 8 and 10m/s as the turbine is operating near peak C_p (Figure 5c). The large decreases at low wind speeds can also be better understood from Figures 5b and 5c, since all the MGF heights cause a more sudden drop-off of C_p to the right of the peak TSR. From analyzing figure 6c it can be noted how the TSR varies for the tested blade configurations, as the controller torque curve settings were not changed. Moreover, TSR is slightly below the design value of 7.5 as 2D C_L and C_D data are used in the inner parts of the rotor blade, as mentioned in section 2.4.

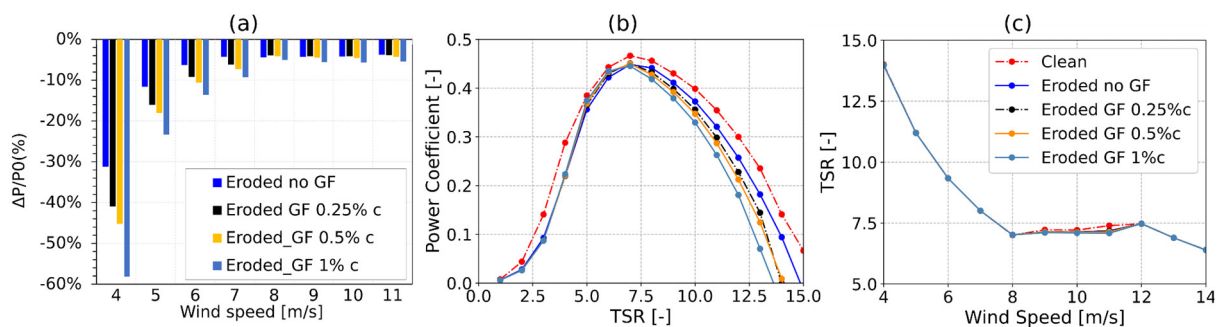


Figure 5. Generator power difference relative to undamaged turbine at various wind speeds (left). Power coefficient as a function of tip-speed ratio (right)

In Figure 6, axial induction factor, angle of attack and tangential force per unit length are shown as a function of blade span at 6 and 9 m/s wind speeds, which correspond to operation at a high and nominal TSR respectively (Figure 5c). The more inner parts of the rotor span are unaffected by erosion, so any difference that may arise in these areas are due to slight differences in rotor speed, while in the outer part of the blade span, important differences between the various simulations can be noted.

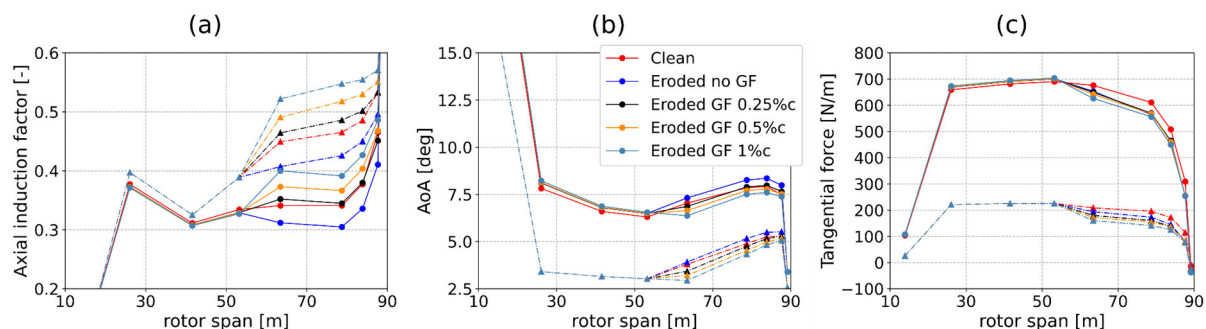


Figure 6. Axial induction Factor (a), Angle of attack (b) and tangential force per unit length (c) along the blade span for various MGF heights. Continuous lines for 9m/s wind speed and dashed lines for 6m/s wind speed.

With respect to the undamaged blade, erosion tends to decrease axial induction. This is caused by the reduction in lift coefficient that can be observed in Figure 4 for the eroded airfoils. On the other hand, when a MGF is applied to the damaged blade, C_L increases with respect to the eroded blade and so does axial induction (Figure 6a). If we focus on the design conditions, with the turbine operating at a mean wind speed of 9 m/s and a TSR near the optimal value, using a MGF with height of 0.25%c on the eroded blade, axial induction is pushed back to a value very close to the undamaged blade's one. This is the desired effect and does lead to a slight performance benefit with respect to the damaged blade (figure 5b). However, as discussed previously and shown in Table 3 and Figure 3, aerodynamic efficiency improves marginally over the damaged airfoil, and remains far from that of the clean blade, thus leading to only small performance gains. When MGFs of 0.5% and 1%c applied, lift coefficient and induction increase beyond the optimum value of 0.33. The higher induction caused by the higher C_L of the blade causes the angle of attack to decrease (Figure 6b) and consequently tangential force to decrease also (figure 6c) due to the consequent reduction in aerodynamic efficiency and a more unfavourable force projection, with Lift will be directed more axially and Drag more tangentially. Both these factors will ultimately contribute to the reduction in power observed. At 6 m/s wind speed on the other hand, the blade is operating at a high TSR (Figure 5c). In these off-design conditions, axial induction of the clean blade is above the optimal value. In his case, the lower C_L caused by the leading edge erosion brings induction closer to its optimal value. Therefore, although the 0.25%c MGF configuration pushes AoA and axial induction back closer to the clean blade, this operating condition is farther from optimum, and thus performance decreases.

4. Conclusions

From an aerodynamic standpoint, the use of MGFs allows for the increase in airfoil efficiency in the presence of leading edge erosion. For the configuration tested herein, the most increases are noted for the 0.5%c MGF height. Overall, however, the increases are comparable to the 0.25%c MGF height configuration, that may be preferable as this MGF should produce less flow unsteadiness. Moreover, the 0.25%c MGF shifts the eroded airfoil lift curve to be very close to the one of the clean blade, which is the target when using these flow devices as a retrofit to an existing blade.

When testing the MGFs as a retrofit device in the current configuration however, the benefits are not obvious. In particular, the only configuration that produced performance increases at nominal TSR is the one with 0.25%c MGF height. In fact, for this configuration, lift coefficient is close to undamaged lift coefficient curve. Therefore, axial induction is also closer to the optimal design value, increasing performance with respect to the eroded blade. Performance increase is however limited as the blade's aerodynamic efficiency remains closer to that of the eroded blade to that of the undamaged one. At high TSRs on the other hand, where the blade often operates at low wind speeds, axial induction is above the optimal design condition even for the reference undamaged blade. In this case, the presence of erosion decreases lift coefficient and as a consequence brings axial induction closer to the optimal design value. Again, MGFs do serve their intended purpose of increasing axial induction to be closer to the original undamaged blade. However, this operating condition is now farther from optimal than the eroded blade, ultimately leading to performance decreases.

As an interesting remark, based on the results presented herein, in order to serve its intended purpose a MGF must be immersed deeply in the boundary layer even in the presence of leading-edge erosion. In fact, the MGFs of 0.5% and 1% chord in height have shown to be too high to be effective on the studied testcase.

In conclusion, MGFs as a retrofit device in the presence of leading edge erosion, if sized correctly, have shown to be able to shift the operating condition of the damaged blade closer to that of the clean undamaged one from an AoA and induction perspective. This leads to slight performance gains in design conditions, but to performance losses with respect to the damaged blade at high TSRs.

References

- [1] Mishnaevsky L, Hasager C B, Bak C, Tilg A-M, Bech J I, Doagou Rad S and Fæster S 2021 Leading edge erosion of wind turbine blades: Understanding, prevention and protection *Renewable Energy* **169** 953–69
- [2] Papi F, Balduzzi F, Ferrara G and Bianchini A 2021 Uncertainty quantification on the effects of rain-induced erosion on annual energy production and performance of a Multi-MW wind turbine *Renewable Energy* **165** 701–15
- [3] Rempel L ROTOR BLADE LEADING EDGE EROSION – REAL LIFE EXPERIENCES 3
- [4] Keegan M H, Nash D H and Stack M M 2013 On erosion issues associated with the leading edge of wind turbine blades *J. Phys. D: Appl. Phys.* **46** 383001
- [5] Bech J I, Hasager C B and Bak C 2018 Extending the life of wind turbine blade leading edges by reducing the tip speed during extreme precipitation events *Wind Energy Science* **3** 729–48
- [6] Sareen A, Sapre C A and Selig M S 2014 Effects of leading edge erosion on wind turbine blade performance: Effects of leading edge erosion *Wind Energ.* **17** 1531–42
- [7] Herring R, Dyer K, Martin F and Ward C 2019 The increasing importance of leading edge erosion and a review of existing protection solutions *Renewable and Sustainable Energy Reviews* **115** 109382
- [8] Bak C, Zahale F and al. 213AD Description of the DTU 10 MW Reference Wind Turbine
- [9] Alber J, Manolesos M, Weinzierl-Dlugosch G, Fischer J, Schönmeier A, Nayeri C N, Paschereit C O, Twele J, Fortmann J, Melani P F and Bianchini A 2021 Experimental investigation of Mini Gurney Flaps in combination with vortex generators for improved wind turbine blade performance *Wind Energy Science Discussions* 1–44
- [10] Drela M 1989 XFOIL: An Analysis and Design System for Low Reynolds Number Airfoils *Low Reynolds Number Aerodynamics* vol 54, ed T J Mueller (Berlin, Heidelberg: Springer Berlin Heidelberg) pp 1–12
- [11] Balduzzi F, Holst D, Melani P F, Wegner F, Nayeri C N, Ferrara G, Paschereit C O and Bianchini A 2021 Combined Numerical and Experimental Study on the Use of Gurney Flaps for the Performance Enhancement of NACA0021 Airfoil in Static and Dynamic Conditions *Journal of Engineering for Gas Turbines and Power* **143**
- [12] Langtry R B and Menter F R 2009 Correlation-Based Transition Modeling for Unstructured Parallelized Computational Fluid Dynamics Codes *AIAA Journal* **47** 2894–906
- [13] Timmer W A and van Rooij R P J O M 2003 Summary of the Delft University Wind Turbine Dedicated Airfoils *Journal of Solar Energy Engineering* **125** 488–96
- [14] Holst D, Church B, Pechlivanoglou G, Tüzüner E, Saverin J, Nayeri C N and Paschereit C O 2017 Experimental Analysis of a NACA 0021 Airfoil Section Through 180-Degree Angle of Attack at Low Reynolds Numbers for Use in Wind Turbine Analysis ASME Turbo Expo 2017: Turbomachinery Technical Conference and Exposition (American Society of Mechanical Engineers Digital Collection)
- [15] National Renewable Energy Laboratory OpenFAST *GitHub*
- [16] Jonkman J M, Hayman G J, Jonkman B J and Damiani R R *AeroDyn v15 User's Guide and Theory Manual* (NREL)